

Research Paper

FTO-mediated autophagy promotes progression of clear cell renal cell carcinoma via regulating SIK2 mRNA stability

Yawei Xu¹, Jingcheng Zhou¹, Lei Li¹, Wuping Yang¹, Zedan Zhang¹, Kenan Zhang¹, Kaifang Ma¹, Haibiao Xie^{1,2}, Zheng Zhang¹, Lin Cai¹, Yanqing Gong¹✉ and Kan Gong¹✉

1. Department of Urology, Peking University First Hospital, Institute of Urology, Peking University, National Urological Cancer Center, Beijing Key Laboratory of Urogenital Diseases (Male) Molecular Diagnosis and Treatment Center, Beijing, China.
2. Department of Urology, Guangdong Provincial People's Hospital, Guangdong Academy of Medical Sciences, Guangzhou, China.

✉ Corresponding authors: **Kan Gong**, Department of Urology, Peking University First Hospital, The Institute of Urology, Peking University, National Urological Cancer Center, Beijing Key Laboratory of Urogenital Diseases (Male) Molecular Diagnosis and Treatment Center, Beijing, 100034, China. E-mail: gongkan_pku@126.com; **Yanqing Gong**, Department of Urology, Peking University First Hospital, The Institute of Urology, Peking University, National Urological Cancer Center, Beijing Key Laboratory of Urogenital Diseases (Male) Molecular Diagnosis and Treatment Center, Beijing, 100034, China. E-mail: yqgong@bjmu.edu.cn.

© The author(s). This is an open access article distributed under the terms of the Creative Commons Attribution License (<https://creativecommons.org/licenses/by/4.0/>). See <http://ivyspring.com/terms> for full terms and conditions.

Received: 2022.08.05; Accepted: 2022.09.19; Published: 2022.10.03

Abstract

The progression of clear cell renal cell carcinoma (ccRCC) remains a major challenge in clinical practice, and elucidation of the molecular drivers of malignancy progression is critical for the development of effective therapeutic targets. Recent studies have demonstrated that N⁶-methyladenosine (m⁶A) is the most abundant modification of eukaryotic mRNA and plays a key role in tumorigenesis and progression. However, the biological roles and underlying mechanisms of m⁶A-mediated autophagy in cancers especially in ccRCC remain poorly elucidated. m⁶A dot blot assay, m⁶A RNA methylation assay kit and immunofluorescence analysis were used to profile m⁶A levels in tissue samples and their correlation with autophagic flux. Expression patterns and clinical significance of fat mass and obesity-associated protein (FTO) were determined through bioinformatics analysis, real-time PCR, western blotting, immunohistochemistry. RNA-seq, MeRIP-seq, MeRIP-qRT-PCR, RIP-qRT-PCR, transmission electron microscopy, immunofluorescence analysis and luciferase reporter assay were used to investigate the underlying mechanism of the FTO-autophagy axis. The role of FTO and autophagy in ccRCC progression was evaluated both *in vitro* and *in vivo*. Here we found that m⁶A modification was suppressed and closely related to autophagic flux in ccRCC. Elevated FTO was inhibited by rapamycin, whereas silencing FTO enhanced autophagic flux and impaired ccRCC growth and metastasis. SIK2 was identified as a functional target of m⁶A-mediated autophagy, thereby prompting FTO to play a conserved and important role in inhibiting autophagy and promoting tumorigenesis through an m⁶A-IGF2BP2 dependent mechanism. Moreover, the small molecule inhibitor FB23-2 targeting FTO inhibited tumor growth and prolonged survival in the patient-derived xenograft (PDX) model mice, suggesting that FTO is a potential effective therapeutic target for ccRCC. Our findings uncovered the crucial role of FTO/autophagy/SIK2 axis in modulating the progression of ccRCC, suggesting that FTO may serve as a valuable prognostic biomarker and promising therapeutic target in ccRCC.

Key words: FTO; autophagy; SIK2; ccRCC

Introduction

Renal cell carcinoma (RCC) is among the ten most common malignancies in both men and women worldwide, accounting for 4.2% of all new cancer cases [1]. The most common histological subtype clear

cell RCC (ccRCC) derives from the epithelial cells of the proximal renal tubule and accounts for most of the cancer-related deaths [2]. It is estimated that over 30% of ccRCC patients present with distant metastasis at

diagnosis. Targeted therapy and immunotherapy improve overall survival, but interindividual variability in treatment response and the resistance that most patients eventually develop leads to a 5-year survival rate of only 8% in patients with metastatic ccRCC [3]. Elucidating the molecular drivers of ccRCC progression and metastasis is critical for the development of effective treatments for advanced ccRCC.

Cancer cells acquire the ability of progression and distant metastasis through genetic and epigenetic changes, one of which is the modification of mRNA transcripts [4]. m⁶A modification affect mRNA stability, subcellular localization, alternative splicing, RNA-protein interactions, transport, translation, and transcription [5]. m⁶A modification play critical roles in the directed differentiation of haematopoietic stem cells, the maintenance of embryonic stem cell pluripotency, the regulation of spermatogenesis, and diseases such as cancer [6]. N⁶-methyladenosine (m⁶A) resulting from methylation modification is the most abundant form of internal RNA modification in eukaryotes. In mammalian cells, m⁶A modification is dynamic and reversible. It is catalyzed by m⁶A methyltransferases (METTL3, METEL14, and WTAP), also known as “writers”. m⁶A demethylases (FTO and ALKBH5), also known as “erasers”, can directly remove m⁶A modifications from mRNA. In addition, specific RNA-binding proteins, also known as “readers”, are responsible for specifically recognizing and binding methylated sites, thereby exerting specific biological functions [7]. FTO (fat mass and obesity-associated protein) is a gene involved in the regulation of adipogenesis and energy intake [8], and its common variants are associated with body mass index and obesity from childhood to the old age [9]. FTO was the first m⁶A demethylase identified among these m⁶A effectors and has been shown to play oncogenic roles in non-small cell lung cancer [10], esophageal squamous cell carcinoma [11], gastric cancer [12], and leukemia [13]. However, the role of RNA methylation in the tumorigenesis and progression of ccRCC remains unclear.

Autophagy is an evolutionarily conserved catabolic degradation mechanism within cells in which cytoplasmic materials, proteins, damaged organelles and lipids are sequestered into vesicles called autophagosomes for degradation and recycling [14]. The mechanism by which FTO regulates autophagy remains unclear. Recently, a study showed that knockdown of FTO resulted in attenuated autophagosome formation, thereby inhibiting autophagy and adipogenesis [8]. Conversely, another study found that silencing FTO in oral squamous cell carcinoma cells increased autophagic flux and

suppressed tumorigenesis [15]. However, the mechanism by which FTO-mediated autophagy regulates ccRCC tumorigenesis and progression is still poorly understood.

In this study, we discovered that FTO was significantly upregulated in ccRCC, and silencing FTO expression increased autophagic flux. Our study reveals that FTO reduces SIK2 mRNA stability through an m⁶A-IGF2BP2-dependent pathway, leading to ccRCC proliferation and metastasis. Taken together, our study suggests a new potential prognostic biomarker and therapeutic target for patients with ccRCC.

Materials and Methods

Patients, specimens and cell culture

This study was based on guidelines of the Declaration of Helsinki and approved by the Institutional Ethical Board of Peking University First Hospital (Beijing, China, BMU2018JI002). All tissue samples were obtained from patients undergoing renal tumor resection at Peking University First Hospital and independently diagnosed as ccRCC by two senior urological pathologists. Between April 2012 to August 2012, 99 pairs of adjacent non-tumor and ccRCC tissue samples were collected for tissue microarray analysis. For ccRCC-1 cohort, tumor tissues and adjacent non-tumor tissues from 99 ccRCC patients who underwent resection between April 2012 to August 2012 were collected to the construction of tissue microarray (TMA). This cohort was used to assess the expression levels and clinical significance of FTO. For ccRCC-2 cohort, RNA was extracted from 24 pairs of frozen adjacent non-tumor and ccRCC tissues for quantitative real-time PCR (qPCR) assay and total RNA m⁶A modification level quantification.

The human ccRCC cell lines (OSRC-2, 786-O, Caki-1, 769-P, ACHN, and A498) and the epithelial cell line of proximal convoluted tubules in human renal cortex (HK2) were purchase from the American Type Culture Collection (ATCC, Manassas, VA, USA). OSRC-2, 786-O, and 769P cells were cultured in RPMI-1640 (Invitrogen-Gibco), and Caki-1, ACHN, A498, and HK2 cells were cultured in DMEM (Gibco). All cells culture media contained 10% fetal bovine serum (Thermo Fisher Scientific) and 1% penicillin-streptomycin (Gibco). All cells were grown at 37°C in a standard humidified incubator with 5% CO₂ and 95% O₂. For function analysis, 10 mM 3MA or 10 μM chloroquine (MedChemExpress) was added to the medium to inhibit autophagy, while 100 nM rapamycin (MedChemExpress) was used to induce autophagy. For the actinomycin D assay, 2 μg/ml actinomycin D (Sigma-Aldrich) was added to OSRC-2

and 786-O cells and the cells were cultured for 0, 6, 12, and 18 hours.

RNA extraction and qRT-PCR

Total RNA was extracted from ccRCC cells and frozen tissues using TRIzol reagent (Invitrogen) and the cDNA was generated by M-MLV reverse transcriptase (Invitrogen) following the manufacturer's instructions. qRT-PCR analysis was performed using SYBR Green PCR Master Mix (Roche) with the Agilent Technologies AriaMx Real-Time PCR System (Agilent). GAPDH served as a normalized internal control and the relative expression of each gene was analyzed using the $2^{-\Delta\Delta C_t}$ method. All primers used in this study are listed in Table S1.

Total RNA m⁶A quantification

Total m⁶A levels in mRNA were detected using the m⁶A RNA methylation assay kit (Abcam) according to the manufacturer's protocol. Briefly, 200 ng of RNA was added to assay wells, followed by the appropriate dilution of detection antibody to each well. The absorbance value at 450 nm was detected by a Varioskan Flash microplate reader (Thermo Scientific, USA), and the relative level of m⁶A RNA methylation in total RNA was calculated according to the following formula: $m^6A\% = [(Sample\ OD - NC\ OD) \div S] / [(PC\ OD - NC\ OD) \div P] \times 100\%$ (S is the amount of input sample RNA in ng, P is the amount of input Positive Control in ng).

m⁶A dot blot assay

The dot blot assay was performed according to the bio-protocol database (<https://en.bio-protocol.org/e2095>). Briefly, RNA samples were spotted onto Amersham Hybond-N+ membranes (GE Healthcare) installed in a Bio-Dot Apparatus (Bio-Rad) followed by UV cross-linking. Stained with 0.02% methylene blue (Solarbio, China) and scanned to indicate the total input RNA content. After drying, the membrane was blocked with 5% BSA for 1 hour and incubated with specific anti-m⁶A antibody (Synaptic Systems, 1:1000) overnight at 4 °C with gentle shaking. Subsequently, the membrane was incubated with HRP-conjugated anti-mouse immunoglobulin G (Abcam, 1:3000) for 1 hour at room temperature. Finally, the membranes were detected with a Chemiluminescent HRP substrate kit (Millipore, USA) and the images were acquired.

Western blot analysis and antibodies

Protein extracts from tissues or cells were obtained by pre-cooled RIPA buffer (Beyotime, Shanghai, China) containing proteases and phosphatases inhibitors (Beyotime, Shanghai, China).

After quantification of protein concentration by BCA assay kit (Pierce), samples were heated at 90 °C for 10 min. Protein abundance was detected and analyzed by SDS-polyacrylamide gel electrophoresis and immunoblotting as described in previous studies [16]. Primary antibodies used in this study were listed in Table S2.

Immunofluorescence analysis

Cells were first washed with phosphate buffered saline (PBS) and fixed with 4% paraformaldehyde for 10 min at room temperature. Permeabilization with Triton X-100 (Beyotime Biotechnology, P0096) for 10 minutes followed by blocking with immunostaining blocking buffer for 1 hour. Subsequently, Cells were incubated with primary antibody overnight at 4 °C, followed by incubation with secondary antibodies. The images were taken by a FV3000 confocal laser microscope (Olympus, Tokyo, Japan). LC3 puncta between 0.3 μM and 1.0 μM in diameter were defined as positive puncta as described in previous studies [8].

Immunohistochemistry (IHC) staining

Tissue samples were fixed in 4% paraformaldehyde overnight and embedded in paraffin. Tissue sections were stained with hematoxylin and eosin (H&E) for histological analysis. The IHC score was calculated by multiplying the staining intensity of cells that stained positively (no staining = 0, weak staining = 1, moderate staining = 2, and strong intense staining = 3) by the score for the percentage of positive cells (no positive staining = 0, 1%-25% = 1, 26%-50% = 2, 51%-100% = 3), resulting in a score range of 0-9. All scoring was performed independently by two senior urologic pathologists.

Plasmids and transfection

Three different lentiviral shRNA oligonucleotide sequences for knockdown of FTO and IGF2BP2, respectively, were synthesized from Syngentech (Beijing, China). Gene sequences coding for FTO, SIK2-WT, and SIK2-MUTs were cloned into the pcDNA3.1 (Invitrogen) vector according to the manufacturer's instructions. The most validated sequences were used for subsequent assays. The transfection of plasmids was performed using Lipofectamine 3000 according to the manufacturer's protocols.

Transmission electron microscopy (TEM)

TEM analysis was performed as described in previous studies [8]. Briefly, cells to be assayed were washed twice with PBS and fixed in 1.5% glutaraldehyde for 4 hours, followed by post-fixed 1% osmium tetroxide for 2 hours. Double-distilled water was used to wash the samples for 5 minutes each

time. Samples were dehydrated in increasing concentrations of ethanol (50%, 70%, 90% and 100%) and anhydrous acetone (3 times, 15 minutes each time). Saturate the samples sequentially with 1:1 and 1:2 mixtures of acetone and embedding medium. The samples were transferred to a 37 °C oven for 12 hours, followed by 48 hours at 60 °C to complete the polymerization procedure. 60 nm ultrathin sections (LEICA EM UC7) stained with 1% uranyl acetate and imaged using a JEM-1400Flash (JEOL, Japan) transmission electron microscope.

Cell proliferation assay

The transfected cells were seeded in 96-well plates at a density of 2000 cells per well with fresh medium. The cell proliferation was detected using CCK8 kit (Dojindo Laboratories, Kumamoto, Japan) at time in 0, 24, 48, 72, and 96 h. The cells were incubated with 10 µl CCK8 reagent at 37 °C for 1h. The absorbance was measured at 450 nm using a Varioskan Flash microplate reader (Thermo Scientific, USA).

Colony formation assay

Seed 500 cells per well in 6-well plates and culture in an incubator for 14 days. Colonies were fixed in 4% paraformaldehyde for 20 minutes and subsequently stained with 0.1% crystal violet (Beyotime, China). Stained colonies were then imaged and manually counted.

Cell migration and invasion assays

In transwell migration and invasion assays, starved ccRCC cells were seeded into the upper chamber (Corning, USA) with (transwell invasion assay) or without (transwell migration assay) Matrigel (BD Biosciences, USA). Medium without fetal bovine serum and ccRCC cells ($1-5 \times 10^4$ cells/200 µl) were added to the upper chamber, and 10% fetal bovine serum was added to the lower chamber medium as the attractant. Cells on the upper surface of the chamber were removed after 24 hours of culture, and cells on the lower surface were fixed with 4% paraformaldehyde and stained in 0.1% crystal violet. Finally, count the stained cells under the microscope.

RNA immunoprecipitation (RIP)-qRT-PCR

RIP assays were performed using Magna RIP Quad RNA-Binding Protein Immunoprecipitation Kit (Merck, USA) according to the manufacturer's protocols. Briefly, cells were lysed with cell lysate containing protease and RNase inhibitors, and cell supernatants were incubated with anti-IGF2BP2 antibody-conjugated beads overnight at 4 °C. The beads were washed with buffer and treated with proteinase K (Beyotime, China) for 1 hour. Then, total

RNA was extracted from the supernatant using TRIzol reagent for qRT-PCR analysis.

MeRIP-seq and MeRIP-qPCR

Total RNA was first extracted from OSRC-2 cells treated with or without 100nM rapamycin for 72h. Fragmented RNA was purified, approximately 1/10 of which was saved as input control, and the remainder was incubated with anti-m⁶A antibody for 2 hours, followed by incubation with ore-washed Protein A/G Magnetic Beads in immunoprecipitation buffer at 4 °C overnight. Subsequently, library preparation and MeRIP-seq was performed by OE Biotech (Shanghai, China) as described in previous studies [17]. For MeRIP-qPCR, a portion of the precipitated product was reverse transcribed by PCR and analyzed.

mRNA stability assays

mRNA stability analysis was performed as described in previous studies [8, 18]. In brief, 5 µg/ml of Actinomycin D (Merck, USA) was used to block cellular mRNA transcription. Cells were harvested after incubation for the indicated times, and total RNA was extracted for reverse transcription. The mRNA transcription level of target gene was detected by qPCR, and the half-life of mRNA was calculated.

Luciferase reporter assay

ccRCC cells were seeded in 6-well plates and cultured to about 70% confluence, then the cells were transfected with plasmids for SIK2-WT or SIK2-MUTs. After 48 hours, measure the luciferase intensity according to the manufacturer's instructions. Luciferase activity was detected by a Dual Luciferase Reporter Gene Assay Kit (KeyGEN BioTECH, China). The Firefly luciferase was used to normalize the activity of Renilla luciferase and to evaluate the expression efficiency.

Orthotopic tumor growth

Animal studies in this study was approved by the Laboratory Animal Ethics Committee of Peking University First Hospital (J2022008, Beijing, China), and all details abide by the ethical principles of laboratory animal welfare and was supervised by the committee and laboratory managers. 6-week-old B-NDG mice (Biocytogen, Beijing, China) were used for orthotopic tumor xenograft assays. Approximately 1×10^6 OSRC-2-lucifer cells stably expressing shCtrl, shFTO or SIK2 were resuspended in 20ul medium containing 2% fetal bovine serum and injected into the kidney capsule of B-NDG mice. When mice were 10 weeks old, they were treated with 3MA at 15 mg/kg/day (i.p.) for 7 consecutive days, and the control group was given vehicle PBS. For intravital

imaging, the mice were anesthetized and injected with 150 mg/kg D-luciferin. Mice were placed into the IVIS-50 chamber (Caliper Life Sciences, USA) in the decubitus or supine position on the affected side. Emissions were collected using filters for green and background fluorescence, and Living Image software (Caliper Life Sciences, USA) was used to process the images. The ratio of fluorescent photon fluxes in the lesion area and the tumor-free background area was recorded, from which the size of the renal tumor was calculated.

Patient-derived xenograft model (PDX model)

B-NDG (Biocytogen, Beijing, China) and BALB/c nude mice (Vital River Laboratory, USA) were used to construct the PDX ccRCC mouse model. Briefly, tumor tissues from two patients undergoing renal tumor resection at Peking University First Hospital were collected and stored at 4 °C in DMEM complete medium. Part of the tumor tissue was taken to make quick-frozen sections, which were identified as ccRCC by two senior urological pathologists. At the same time, tumor tissue was shredded to 1-3 mm³ and then implanted subcutaneously in the abdomen of B-NDG mice. When PDX tumors grew to 1-2 cm³, the tumor tissue was chopped and transplanted into the next generation of mice. The fourth generation of PDX-bearing mice started treatment with FE23-2 (MedChemExpress, USA) when tumors reached 50 mm³ as described previously [19]. FE23-2 at 8 mg/kg/day (i.p.) was administered continuously for 14 days, and the control group was administered with vehicle DMSO. To ensure a consistent therapeutic dose of 6 mg/kg/day, mice were weighed daily during treatment and the dose received was recalculated. Mice were euthanized 6 weeks after the end of treatment, kidney tumors were dissected and collected for further analysis, and tumor volume and weight were recorded.

Statistical analysis

Statistical analyses were performed using SPSS v23.0 (IBM Corp., Armonk, NY, USA) or GraphPad Prism v7.0 (GraphPad Software, La Jolla, CA, USA). Data are presented as the mean ± standard error of the mean (SEM). Univariate and multivariate Cox regression analyses were performed to examine independent factors, Pearson's test was used to assess correlation between different groups. A *p* value of < 0.05 was considered significant.

Results

m⁶A modification levels are decreased and closely correlated with autophagy in ccRCC

To determine the functional roles of m⁶A

modification in ccRCC, we first measured the m⁶A RNA levels in 24 human ccRCC tissues and paired adjacent noncancerous tissues (ANCT). We found that the m⁶A levels were significantly lower in ccRCC than in ANCT via a dot blot assay (Fig. 1a). The results were also confirmed by the m⁶A RNA methylation quantification kit (Fig. 1b). Furthermore, we evaluated the relationship between m⁶A levels and clinicopathology and observed remarkably decreased m⁶A levels in T stage 3-4 than in T stage 1-2 (Fig. 1c), and the m⁶A levels were also decreased in stage II-III than in stage I (Fig. 1d). OSRC-2-luciferase cells were orthotopically injected into immunodeficient B-NDG mice (Fig. 1e), we found that m⁶A levels decreased in the higher photon flux group in the renal tumors (Fig. 1f), and they also decreased in lung metastases (Fig. 1g).

To analyze the correlation between autophagy and m⁶A RNA methylation in ccRCC, we established cellular models of rapamycin-induced autophagy. The m⁶A modification levels were significantly increased in the ccRCC cell lines OSRC-2 and 786-O after treatment with rapamycin (Fig. 1h-i). GFP signal is easily quenched in acidic autolysosomes, while RFP is more stable. Autophagosome and lysosome fusion occurs when GFP and mRFP fluorescence co-localize, resulting in the loss of yellow puncta and the appearance of only red puncta. Therefore, a green fluorescent protein (GFP)-monomeric red fluorescent protein (mRFP)-LC3B construct was used to determine the correlation between m⁶A RNA methylation and autophagic flux in ccRCC cell lines (Fig. S1, Fig. 1j). Correlation analysis revealed that autophagic flux and m⁶A levels were positively correlated in ccRCC cells (Fig. 1k). Together, these results suggest that m⁶A modification levels are significantly decreased and closely related to its autophagic flux in ccRCC.

Elevated FTO expression correlates with poor prognosis of patients with ccRCC

To identify potential target genes of m⁶A RNA methylation in autophagy, we first employed qPCR analysis to compare the mRNA expression of m⁶A-related effectors (METTL3, METTL14, METTL16, WTAP, VIRMA, ZC3H13, RBM15, RBM15B, YTHDC1, YTHDC2, YTHDF1, YTHDF2, YTHDF3, HNRNPC, FMR1, LRPPRC, HNRNPA2B1, IGFBP1, IGFBP2, IGFBP3, RBMX, FTO, and ALKBH5) following rapamycin treatment. Our results showed that the mRNA levels of IGFBP2, FTO, and ALKBH5 were significantly attenuated after rapamycin treatment (Fig. 2a), while only FTO was also markedly downregulated at protein levels by rapamycin treatment (Fig. 2b and Fig. S2).

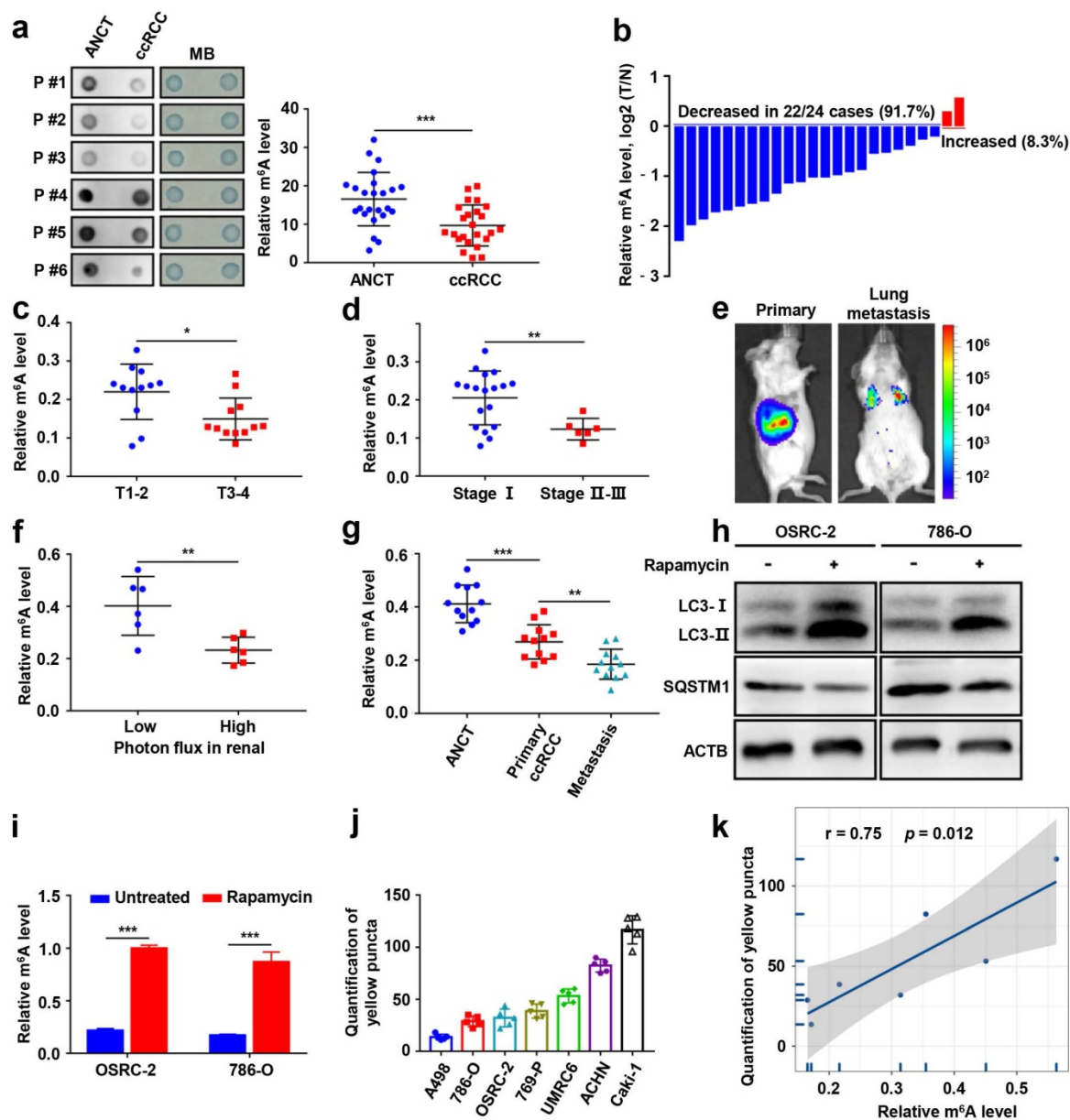


Figure 1. m6A modification levels are decreased and closely correlated with autophagy in ccRCC. a) The mRNAs isolated from ccRCC tissues and paired adjacent noncancerous tissues (ANCT) were used in dot blot analyses with an anti-m⁶A antibody, and MB (methylene blue) staining served as the loading control (representative images in the left panel), and the relative m⁶A RNA levels were calculated (right panel, n=24). b) The m⁶A RNA levels in the same 24 ccRCC tissues and paired ANCT were detected by the m⁶A RNA methylation quantification kit. c) The m⁶A RNA levels in T stage I-2 versus T stage 3-4 of ccRCC tissues by the m⁶A RNA methylation quantification kit. d) The m⁶A RNA levels in stage I versus stage II-III of ccRCC tissues by the m⁶A RNA methylation quantification kit. e) Representative images of orthotopic transplantation and lung metastasis mouse model. f) Quantification of m⁶A levels in two groups with low and high photon flux of orthotopic tumor in mouse kidney by the m⁶A RNA methylation quantification kit. g) Quantification of m⁶A levels in ANCT, primary ccRCC, and lung metastases by the m⁶A RNA methylation quantification kit. h-i) LC3- I/II and SQSTM1 expression in OSRC-2 and 786-O cells treated with or without 100nM rapamycin for 72 hours using western blot analysis and the m⁶A levels in the total mRNA was determined using an m⁶A RNA methylation quantification kit. j) Quantification of LC3 puncta. k) Relationship between relative m⁶A RNA levels and autophagy in ccRCC cell lines. Error bars, SEM; *, P < 0.05; **, P < 0.01; ***, P < 0.001.

Having identified FTO as a potential target of m⁶A RNA methylation in autophagy, we sought to further assess FTO expression in ccRCC and ANCT. Bioinformatics analysis of 539 ccRCC samples and 72 adjacent noncancerous samples from The Cancer Genome Atlas (TCGA) database revealed significantly increased FTO expression in ccRCC tissues compared to ANCT (Fig. 2c). Subsequently, we analyzed two GEO datasets, GSE53757 and GSE66271, which also suggested that FTO is elevated in ccRCC compared to ANCT (Fig. 2d-e). Furthermore, we examined FTO

expression in eight pairs of ccRCC tissues and ANCT, which further verified that FTO was significantly increased in ccRCC compared to ANCT at mRNA levels (Fig. 2f). In all eight pairs, the protein levels of FTO were found to be higher in human ccRCC tissues than in their ANCT by western blot (Fig. 2g). These results were confirmed in a ccRCC tissue microarray containing 30 pairs of ccRCC and adjacent tissue, which showed that FTO protein levels were increased in ccRCC tissue compared with that in ANCT by IHC staining (Fig. 2h). Additionally, the data showed that

patients with high FTO expression had poorer overall 10-year survival than those with low FTO expression (n=39, p<0.05, log-rank test; Fig. 2i). Simultaneously, univariate and multivariate Cox regression revealed that high FTO expression was an independent prognostic factor for overall survival (OS) (HR=1.63, 95% CI: 1.06-2.52; p=0.026) in ccRCC (Fig. 2j). To further examine the predictive power of FTO expression levels in the OS of ccRCC patients, we performed a time-dependent receiver operating

characteristic curve analysis and found that when FTO expression levels was combined with other clinical variables, its predictive efficiency was much better than either alone (Fig. S2). Taken together, these data suggest that FTO is elevated in ccRCC and may be related to autophagic flux in rapamycin-treated ccRCC cells, and its expression level might be an independent prognostic factor for patients with ccRCC.

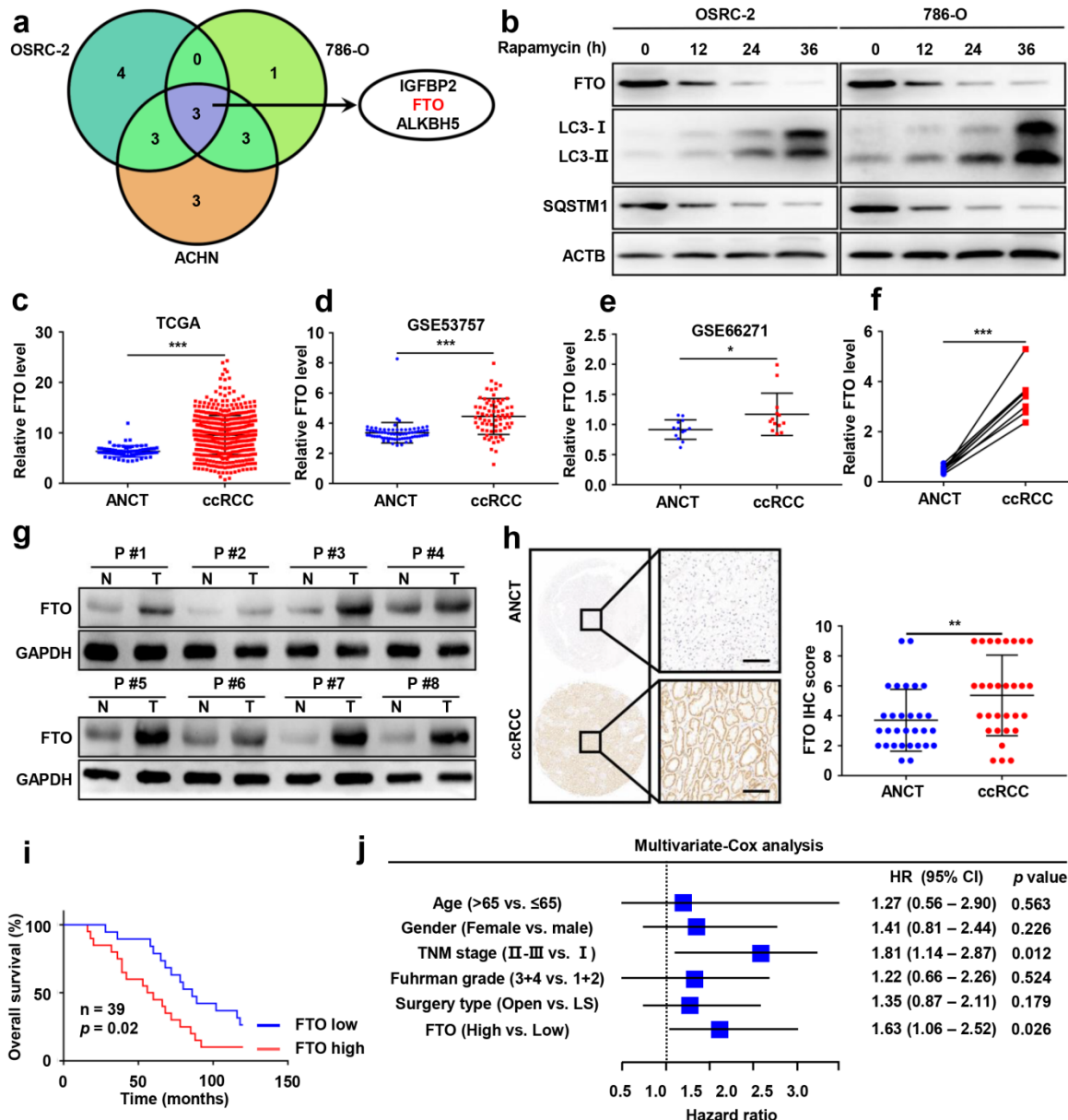


Figure 2. Elevated FTO expression correlates with poor prognosis of patients with ccRCC. a) A venn diagram of differentially expressed m⁶A-related genes in three ccRCC cell lines treated with 100nM rapamycin for 72 hours. b) FTO, LC3- I/II, and SQSTM1 expression in OSRC-2 and 786-O cells treated with rapamycin at 0, 12, 24, and 36 h, measured using western blot analysis. c) FTO mRNA expression in 539 ccRCC tumor tissues as compared to 72 adjacent noncancerous tissues (ANCT) from TCGA data. d) FTO mRNA expression in 72 paired ccRCC tumor tissues and ANCT from GSE53757 GEO datasets. e) FTO mRNA expression in 13 paired ccRCC tumor tissues and ANCT from GSE66271 GEO datasets. f-g) Real-time PCR and western blot analysis of FTO expression in 8 paired ccRCC tumor tissues and ANCT. h) Immunohistochemical (IHC) analysis of FTO in a ccRCC tissue microarray (TMA) 30 ccRCC tumor and ANCT pairs (left panel, scale bar, 100 μm) and quantification of FTO expression by IHC analysis in ccRCC TMA samples as compared to ANCT (right panel). i) Kaplan-Meier overall survival (OS) analysis of FTO expression in patients with ccRCC (log-rank test). j) Multivariable analyses were performed in the ccRCC cohort. All bars correspond to 95% CIs. Error bars, SEM; *, P < 0.05; **, P < 0.01; ***, P < 0.001.

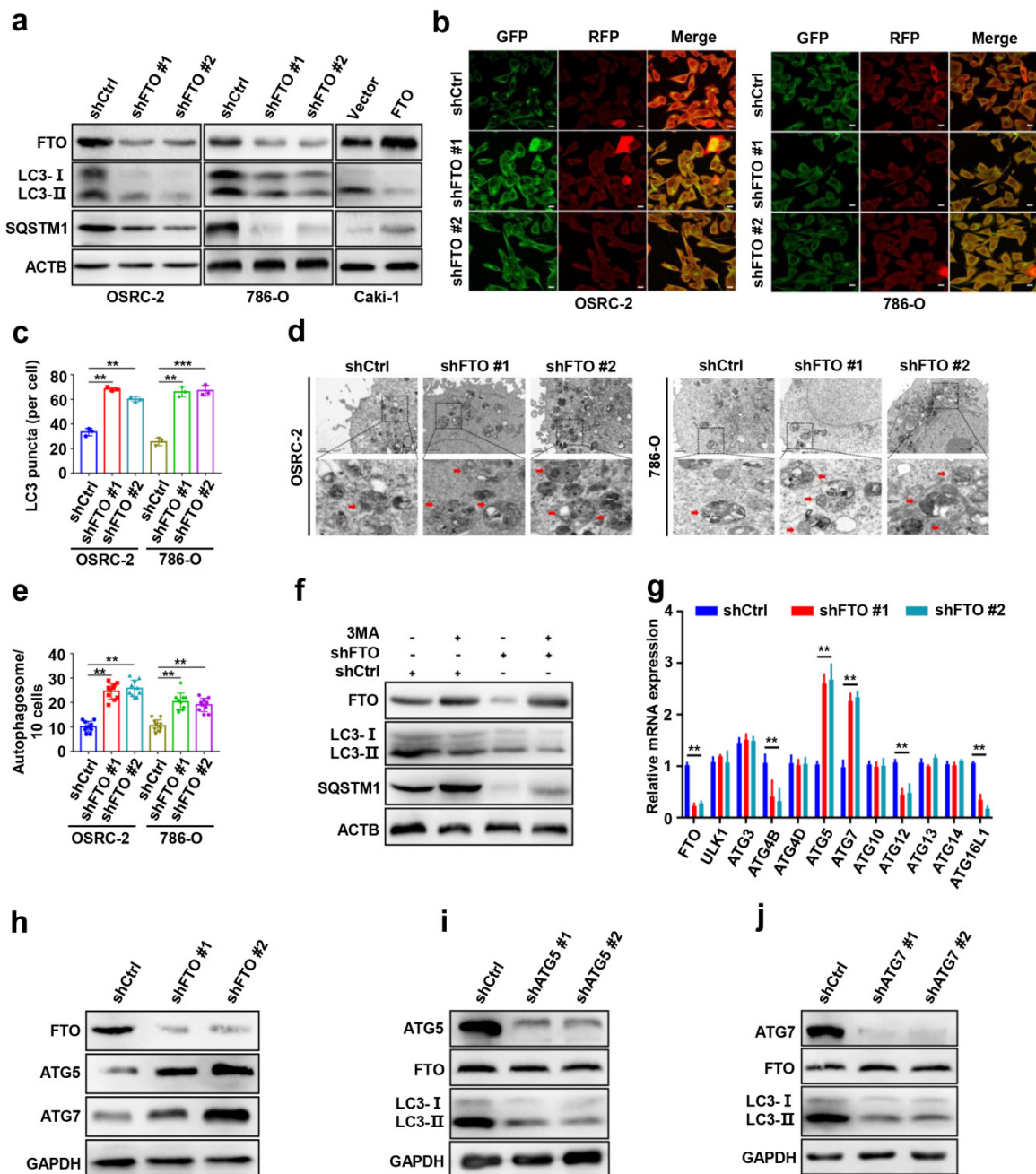


Figure 3. FTO downregulation enhances ccRCC autophagic flux by targeting ATG5 and ATG7. a) Plasmids containing FTO shRNA and FTO were transfected into OSRC-2, 786-O, or Caki-1 cells to establish stable cell lines. Western blot analysis was used to detect FTO, LC3- I/II, and SQSTM1 expression. b-c) IF staining with mRFP-GFP-LC3 in OSEC-2 and 786-O cells with FTO knockdown. Red puncta signify autolysosomes and yellow puncta signify autophagosomes and quantification of LC3 puncta. Scale bar, 10 μ m. d-e) Transmission electron microscopy (TEM) demonstrating autophagosomes in OSRC-2 and 786-O cells with FTO knockdown, and quantification of autophagosomes in cells. Arrows indicate autophagosomes. Scale bar: 0.5 μ m. f) Western blotting analysis of FTO, LC3- I/II, and SQSTM1 expression in control and FTO knockdown cells treated with or without 10 mM 3MA for 6h. g) qPCR analysis of expression levels of autophagy-related proteins in control and FTO knockdown cells. Actb was used as an internal control. h) Western blotting analysis of FTO, ATG5, and ATG7 expression in control and FTO knockdown cells. ACTB was used as a loading control. i) Western blotting analysis of ATG5, FTO, and LC3-I/II expression in control and ATG5 knockdown cells. j) Western blotting analysis of ATG7, FTO, and LC3-I/II expression in control and ATG7 knockdown cells. Error bars, SEM; $P < 0.01$; $***, P < 0.001$.

FTO downregulation enhances ccRCC autophagic flux by targeting ATG5 and ATG7

To further explore the role of FTO in autophagy, we first silenced FTO in ccRCC cell lines using independent FTO short hairpin RNAs (shRNAs) in OSRC-2, and 786-O cells. The protein levels of microtubule-associated protein 1 light chain 3-beta (MAP1LC3B/LC3, an autophagy activation marker),

and SQSTM1/p62 were measured by western blot to confirm that autophagy activation of cells had occurred (Fig. 3a). Silencing of FTO significantly increased the ratio of LC3-II: I and decreased SQSTM1 levels compared to control cells, suggesting a steady-state autophagosome formation (Fig. 3a). Immunofluorescence assays showed that more LC3 puncta were formed after FTO silencing in OSRC-2 and 786-O cells (Fig. 3b-c). Additionally, we also

analyzed autophagosome formation by TEM and found that silencing of FTO increased the number of autophagosomes, indicating upregulated activation of autophagy (Fig. 3d-e). To confirm whether autophagy was affected by FTO deficiency, FTO-deficient and control cells were treated with or without 3-MA (an alternative autophagy inhibitor). We observed that 3-MA treatment of cells not only attenuated autophagy, but also increased FTO protein expression (Fig. 3f). These findings suggest that FTO negatively modulates autophagy activation in ccRCC cells.

To screen potential target genes of FTO in autophagy, we first compared the mRNA expression differences of autophagy-related genes following FTO deficiency by qPCR assays. The results showed that the mRNA levels of Atg5 and Atg7 were markedly increased following FTO deficiency (Fig. 3g). Consistently, FTO deficiency significantly upregulated ATG5 and ATG7 at protein levels (Fig. 3h). To further determine the upstream-downstream relationship between FTO and ATG5 and ATG7, we knocked down Atg5 and Atg7 in OSRC-2 cells, respectively. The knockdown efficiency was verified by western blot (Fig. 3i-j). The data showed that the LC3-II: I ratio markedly decreased following Atg5 and Atg7 depletion while FTO protein expression did not change, indicating that FTO was upstream of ATG5 and ATG7 (Fig. 3i-j). Collectively, these results confirmed that FTO downregulation may enhance autophagic flux by targeting ATG5 and ATG7.

FTO downregulation impairs ccRCC growth *in vitro* and *in vivo*

To examine the function of FTO in ccRCC, we conducted Cell Counting Kit-8 (CCK8) proliferation assays and 2D clonogenic assays in OSRC-2 and 786-O cells. FTO downregulation significantly attenuated the proliferation and 2D colony formation, whereas the inhibitory effect of silencing FTO on the malignant behavior of ccRCC cells was partially relieved by 3-MA treatment (Fig. 4a-d). Furthermore, we assessed the effect of FTO on ccRCC growth *in vivo*. OSRC-2-luciferase cells with knockdown of FTO and corresponding control cells were orthotopically injected into immunodeficient B-NDG mice. Tumor growth was impaired in FTO downregulation mice compared to WT mice, as illustrated by bioluminescence imaging (Fig. 4e). We observed that decreased FTO expression inhibited tumor growth (volume and weight, Fig. 4f-i) and Ki67 staining (Fig. 4j) in orthotopic transplantation models in B-NDG mice. Consistently, tumors showed decreased proliferation following FTO downregulation, but this inhibitory was partially relieved by 3-MA treatment (Fig. 4e-j). These data suggest that FTO deficiency

impairs ccRCC growth *in vitro* and *in vivo*, and that this inhibitory function is partially alleviated by autophagy-inhibitory treatment.

FTO downregulation impairs ccRCC metastasis *in vitro* and *in vivo*

To examine the roles of FTO in ccRCC metastasis, we first conducted migration and invasion assays *in vitro*. The results showed that downregulated expression of FTO impaired the migration and invasion of OSRC-2 and 786-O cells (Fig. 5a-b). Subsequently, we further evaluate the effect of FTO on ccRCC metastasis *in vivo*. After four weeks, downregulation of FTO significantly impairs ccRCC lung metastasis (Fig. 5c) and the number of lung metastatic lesions (Fig. 5d) compared with those in control groups, and this inhibitory was partially relieved by 3-MA treatment. Moreover, FTO knockdown in these ccRCC cells significantly prolonged the overall survival in mice with lung metastases ($p=0.0004$), and this effect was partially attenuated following 3-MA treatment ($p=0.0286$, Fig. 5e). Compared with the control group, the N-cadherin IHC score decreased in the FTO downregulated group, whereas the E-cadherin IHC score increased, which were partially reversed by 3MA treatment (Fig. 5f-g). These data suggest that FTO deficiency impairs ccRCC metastasis *in vitro* and *in vivo*, and that this inhibitory function is partially alleviated by autophagy-inhibitory treatment.

Identification SIK2 as the functional target of m⁶A-mediated autophagy in ccRCC cells

To identify potential mRNA targets of m⁶A modification, OSRC-2 cells undergoing rapamycin-induced autophagy were selected for methylated RNA immunoprecipitation sequencing (MeRIP-seq) and RNA sequencing (RNA-seq). The data showed that 512 genes were upregulated and 384 genes were downregulated after rapamycin-induced autophagy (Fig. 6a). MeRIP-seq identified 14554 and 14825 m⁶A peaks, of which 1374 and 1399 were unique in the control cells and cells with autophagy induction, respectively (Fig. 6b). Consistent with previous studies [20], the most common m⁶A motif, GGAC was highly enriched in the m⁶A peaks (Fig. 6c). Notably, these m⁶A modification were mainly enriched in the coding region (CDS) and 3'-untranslated region (3'-UTR) (Fig. 6d, Fig. S3). Gene Ontology and Kyoto Encyclopedia of Genes and Genomes pathway analyses demonstrated that the differentially expressed genes were associated with biological adhesion, biological regulation, growth, environment adaptation, and nucleotide metabolism (Fig. S4). To identify potential targets of m⁶A in the regulation of

autophagy, we comprehensively analyzed RNA-seq and MeRIP-seq data. We compared genes with differential expression and m⁶A enrichment in our MeRIP-seq and RNA-seq datasets from the control and cells undergoing rapamycin-induced autophagy, and with differential expression of human matched primary ccRCC and metastasis (GSE85258 [21] and GSE23629 [22]), generated from previous studies. We observed that three genes SIK2, PIK3C2A, and RNF34, appeared in the overlapping region of the above four datasets (Fig. 6e). In addition, SIK2, PIK3C2A and RNF34 were hypermethylated-upregulated (Fig. 6f). Furthermore, we examined the mRNA levels of SIK2, PIK3C2A, and RNF34 in 3-MA treated OSRC-2 cells

and found that SIK2 was markedly upregulated, while PIK3C2A and RNF34 were not changed (Fig. 6g). Consistently, SIK2 protein levels decreased following 3-MA treatment (Fig. 6h). Our MeRIP-seq data revealed that the m⁶A abundance in the SIK2 mRNA was markedly increased during autophagy flux (Fig. S5). To further validate m⁶A methylation in SIK2 mRNA, we conducted methylated RNA immunoprecipitation quantitative PCR (MeRIP-qPCR). As expected, MeRIP-qPCR assay analysis showed that the m⁶A modification level of SIK2 mRNA was significantly increased after autophagy activation (Fig. 6i).

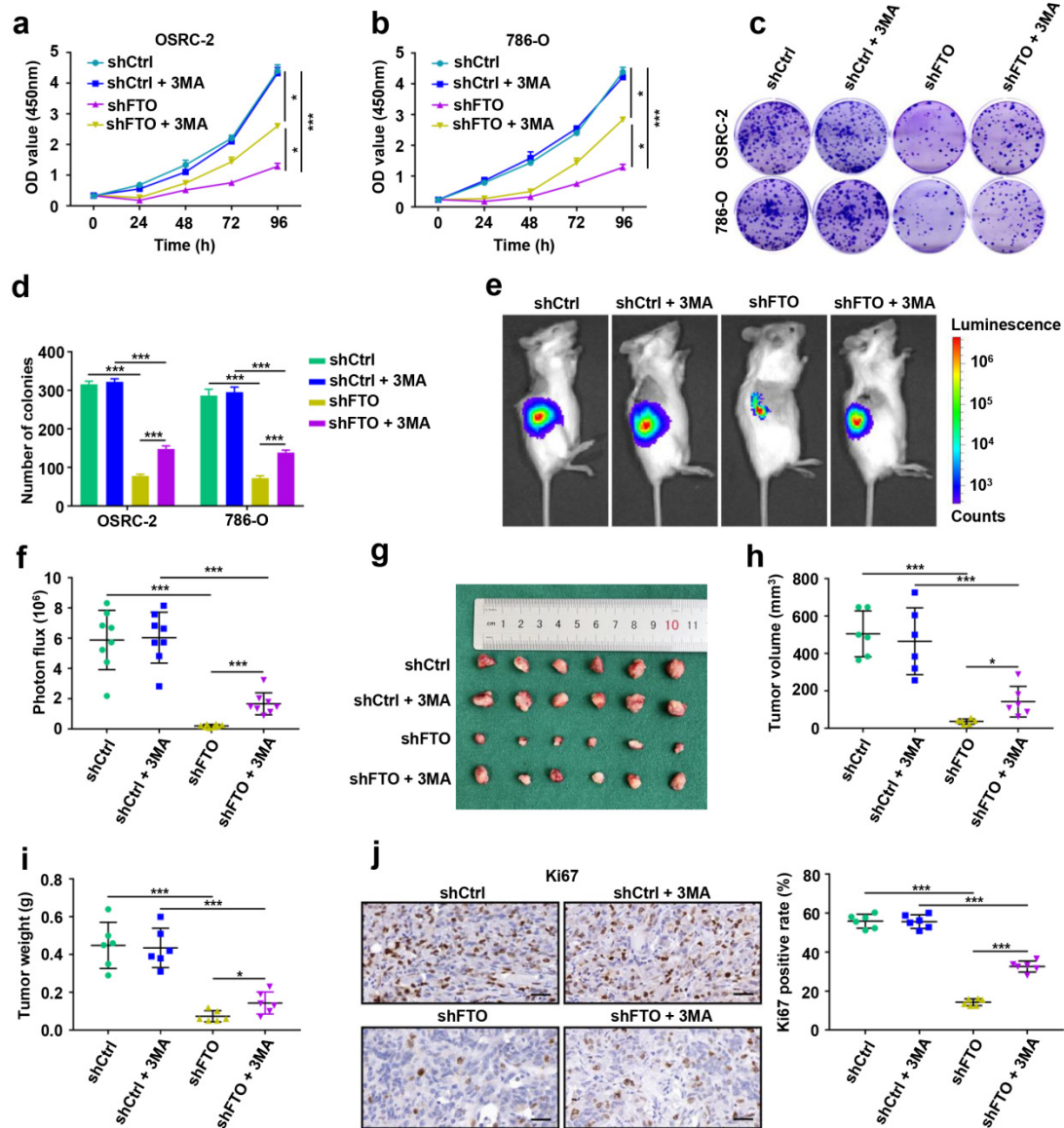


Figure 4. FTO downregulation impairs ccRCC growth *in vitro* and *in vivo*. a-b) Viability of OSRC-2 and 786-O cells (shCtrl and shFTO, treated with or without 10 mM 3MA) detected using the CCK8 assay. c-d) Representative images from the colony-forming assay and colony number analysis. All experiments were performed in triplicate and data were presented as the mean ± SD. e) Representative images of the orthotopic transplantation mouse model (shCtrl and shFTO, treated with or without 3MA). f) The analysis of the orthotopic tumor photon flux. g) Image of orthotopic transplanted tumors from the indicated groups. h-i) Tumors were removed 8 weeks after orthotopic transplantation, followed by volume calculation and weight measurement. j) Representative IHC staining images of Ki67 (scale bar, 100 μm, left panel) and quantification of Ki67 positive rate (right panel). Error bars, SEM; *, P < 0.05; ***, P < 0.001.

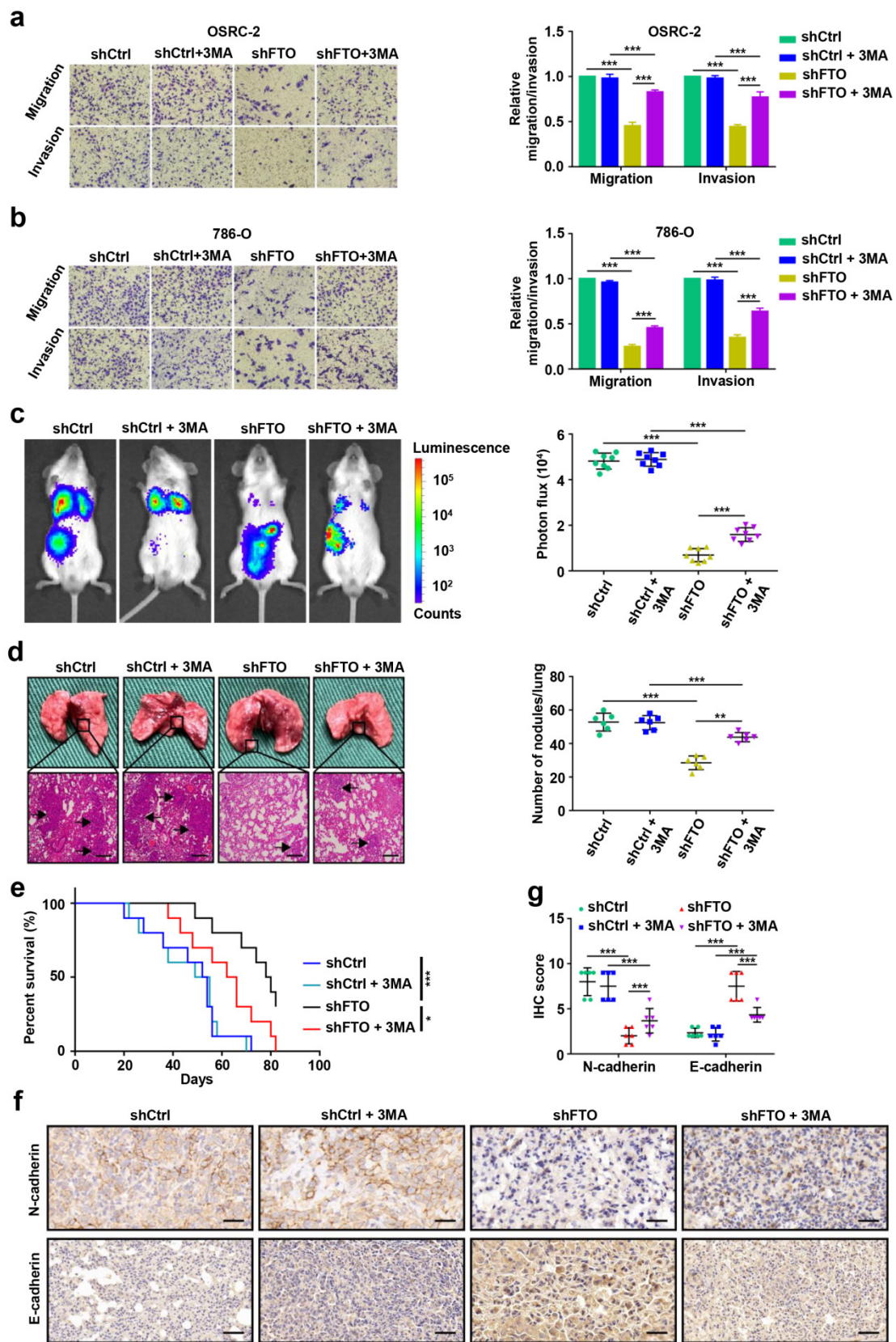


Figure 5. FTO downregulation impairs ccRCC metastasis *in vitro* and *in vivo*. **a-b**) Cell migration and invasion assays of OSRC-2 and 786-O cells after knockdown of FTO (treated with or without 10 mM 3MA). Representative images (left panel) and quantification (right panel) of the cell migration and invasion assay results were shown. **c**) Representative images of the orthotopic transplantation lung metastasis mouse model (shCtrl and shFTO, treated with or without 3MA; left panel), and the analysis of the lung metastasis photon flux (right panel). **d**) Representative images of metastatic lung tumors and hematoxylin and eosin (H&E) staining (left panel), and quantification of lung tumors (right panel). **e**) The survival of mice orthotopically transplanted with control or knockdown FTO OSRC-2 cells was documented (n=10 mice per group). **f-g**) Representative IHC staining images of N-cadherin and E-cadherin (scale bar, 100 μ m) and quantification of IHC score. Error bars, SEM; *, $P < 0.05$; **, $P < 0.01$; ***, $P < 0.001$.

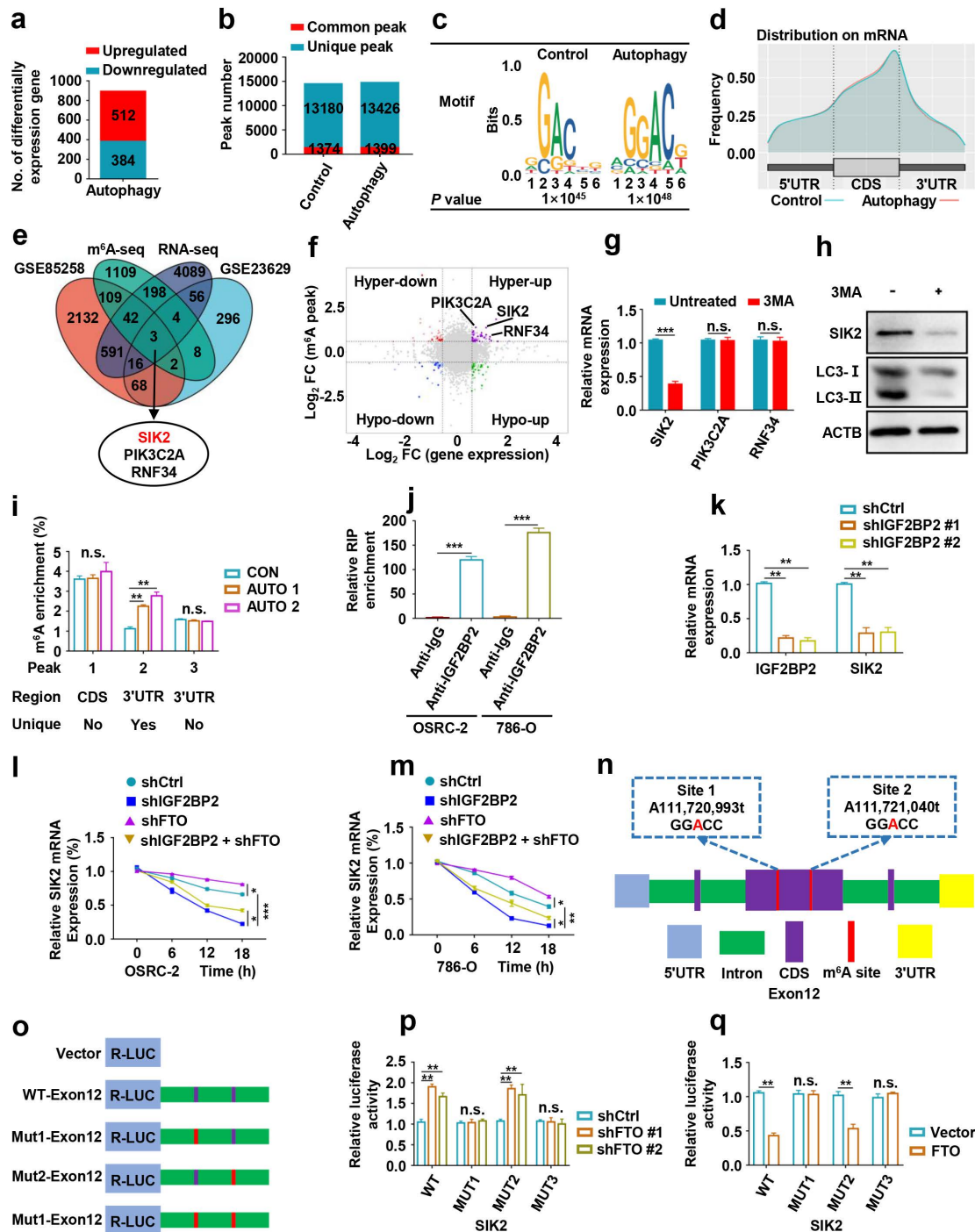


Figure 6. Identification SIK2 as the functional target of m⁶A-mediated autophagy in ccRCC cells. a) Differentially expressed genes with over 2-fold expression changes in OSRC-2 cells treated with or without 100nM rapamycin for 72 hours. b) Number of common and unique m⁶A peaks from MeRIP-seq. c) Top consensus motif identified from MeRIP-seq. d) Metagene profiles of m⁶A enrichment across mRNA transcriptome. e) A venn diagram of FTO-mediated autophagy downstream analysis. f) Localization of SIK2, PIK3C2A, and RNF34 in the quadrant chart of the distribution of peaks. g) SIK2, PIK3C2A, and RNF34 mRNA expression with or without 10 mM 3MA for 6h. h) Western blotting analysis of SIK2 and LC3- I/II expression in control and FTO knockdown cells treated with or without 10 mM 3MA for 6h. i) MeRIP-qPCR analysis of SIK2 RNA from OSRC-2 cells (treated with or without rapamycin). j) RNA immunoprecipitation (RIP)-qPCR assay using IGF2BP2-specific antibody and IgG control antibody to detect the enrichment of IGF2BP2 binding to SIK2 m⁶A modification sites. k) qPCR analysis of SIK2 and IGF2BP2 in OSRC-2 cells (control and IGF2BP2 depleted). l-m) RNA stability analysis of SIK2 mRNA levels in OSRC-2 and 786-O cells (control or IGF2BP2 depleted) in the absence or presence of FTO silencing, and after actinomycin D treatment. n) Location of the m⁶A site in the SIK2 mRNA sequence. o) Schematic diagram of dual-luciferase reporter constructs. p-q) Relative luciferase activity of WT or MUT (A-to-T mutation) SIK2 luciferase reporter in control, FTO knockdown and FTO overexpressing cells. Error bars, SEM; *, P < 0.05; **, P < 0.01; ***, P < 0.001.

Studies have shown that m⁶A methylation modification on mRNA affect mRNA stability, which is mediated by specific m⁶A-binding proteins [8, 23, 24]. As a main m⁶A “reader”, IGF2BP2 (Insulin-like growth factor 2 mRNA-binding protein 2) has been

reported to promote the tumor progression by selectively recognizing and stabilizing m⁶A-modified mRNA [25]. The IGF2BP2-specific antibody markedly enriched SIK2 mRNA in the RNA immunoprecipitation-qPCR assay compared to the IgG control

antibody, indicating that IGF2BP2 binds SIK2 mRNA (Fig. 6j). To determine whether IGF2BP2 is a potential reader for SIK2 m⁶A methylation, we knocked down IGF2BP2 and observed strongly decreased expression of SIK2 in ccRCC cells (Fig. 6k). IGF2BP2 knockdown not only increased SIK2 mRNA stability and expression levels, but also abolished the attenuation caused by FTO silencing when the transcription was blocked with actinomycin D (Fig. 6l-m).

Next, we assessed whether FTO and IGF2BP2-mediated regulation is necessary for m⁶A modification on target mRNAs. Among the m⁶A peaks in our MeRIP-seq dataset, the multiple m⁶A peaks in exon 12 are more consistent and contain two GGAC motifs (Fig. 6n). We performed dual luciferase reporter and mutagenesis assays and generated five luciferase reporters including Renilla luciferase, wild-type, mutant 1, mutant 2, and mutant 3 of SIK2 exon2 (A was replaced by T in GGAC) (Fig. 6o). The luciferase assays revealed that FTO downregulation could increase the luciferase activity of the reporter construct bearing wild-type and mutant 2, but not mutant 1 and mutant 3 (Fig. 6p). Consistent results were observed when cells were co-transfected with plasmids overexpressing FTO and luciferase (Fig. 6q). Together, our findings indicate that FTO-mediated m⁶A modification regulates SIK2 expression via IGF2BP2-dependent SIK2 mRNA stability.

Effects of FTO-mediated SIK2 on autophagic flux, progression and survival in ccRCC

To explore the role of SIK2 in ccRCC, we overexpressed SIK2 and found that autophagic flux was enhanced, suggesting that autophagy was activated (Fig. 7a-b). To further clarify the underlying molecular mechanism by which FTO regulates autophagy, we constructed the wild-type (FTO-WT) and catalytic mutant FTO^{R96Q} (FTO-MUT) plasmids to determine whether the demethylase activity of FTO was required [8, 26]. The effect of ectopic expression of FTO-WT or FTO-MUT on the total cellular m⁶A level was confirmed by the m⁶A RNA methylation quantification kit (Fig. 7b-c). Upregulation of FTO-WT reversed SIK2 expression and increased LC3-II: I ratio, but FTO-MUT failed for both, indicating that the demethylase activity of FTO is involved in this mechanism (Fig. 7b). Furthermore, we analyzed autophagosome formation by TEM and found that SIK2 upregulation increased the number of autophagosomes, but the ectopic expression FTO or 3-MA treatment reversed the enhanced autophagy (Fig. 7d-e).

Moreover, overexpression of SIK2 in OSRC-2 and 786-O cells resulted in decreased in both proliferation (Fig. 7f-h), migration, and invasion (Fig.

7i-j). However, 3-MA treatment or FTO upregulation partially reversed these effects. Results of orthotopic injected ccRCC models showed significantly lower photon flux of tumors in the SIK2 overexpression group at the third week compared to the control group (Fig. 7k-l). Noticeably, SIK2 overexpression group mice had smaller tumor volume (Fig. 7m-n) and tumor weight (Fig. 7o) with decreased Ki67 staining compared with control mice (Fig. 7p-q). Consistently, SIK2 overexpression group mice had fewer lung metastasis photon flux (Fig. 7r) and the number of lung metastatic nodules (Fig. S6) compared with those in control groups. As expected, overexpression of SIK2 markedly prolonged overall survival in ccRCC mice (Fig. S7). Compared with the control group, the N-cadherin IHC score decreased in the SIK2 ectopic expression group, whereas the E-cadherin IHC score increased (Fig. S7). Together, these results demonstrate that FTO-mediated SIK2 can promote autophagic flux and the enforced expression of SIK2 efficiently inhibits the progression and survival of ccRCC *in vitro* and *in vivo*.

Small-molecule inhibitor targeting FTO exhibits therapeutic efficacy in a PDX ccRCC mouse model

Several FTO small-molecule inhibitors such as FB23-2 [6], Dac51 [27], R-2HG [28], and CS1/CS2 [29] have been reported to inhibit the demethylation activities of FTO. Recently, a study showed that the FTO small-molecule inhibitor FB23-2 directly binds FTO and selectively inhibits m⁶A demethylase activity [6]. More importantly, FB23-2 dramatically inhibited the progression of human acute myeloid leukemia cell lines and primary cells in xenografted mice [6], highlighting the broad potential of targeting FTO for cancer therapy. However, the anticancer effect of FB23-2 on solid tumors including ccRCC is unclear. Therefore, we applied FB23-2 in the PDX model to validate whether FTO is a druggable target of ccRCC. We generated ccRCC PDX murine models (Fig. 8a), and the clinicopathological characteristics of the donor patients are shown in Fig. 8b-c. Results revealed that mice in the FB23-2-treated group had smaller tumor volume and tumor weight (Fig. 8d-g), as well as a longer survival benefit (Fig. 8h-i), compared to control mice. IHC staining confirmed decreased FTO expression in the FB23-2 treatment group and increased SIK2 expression in the control group (Fig. 8j-k). The Ki67 expression level was dramatically decreased in the FB23-2 treated group compared with the control group (Fig. 8j-k). Collectively, our data suggest that FTO is a druggable target and that FB23-2, a small molecule inhibitor targeting FTO, have the potential to treat ccRCC.

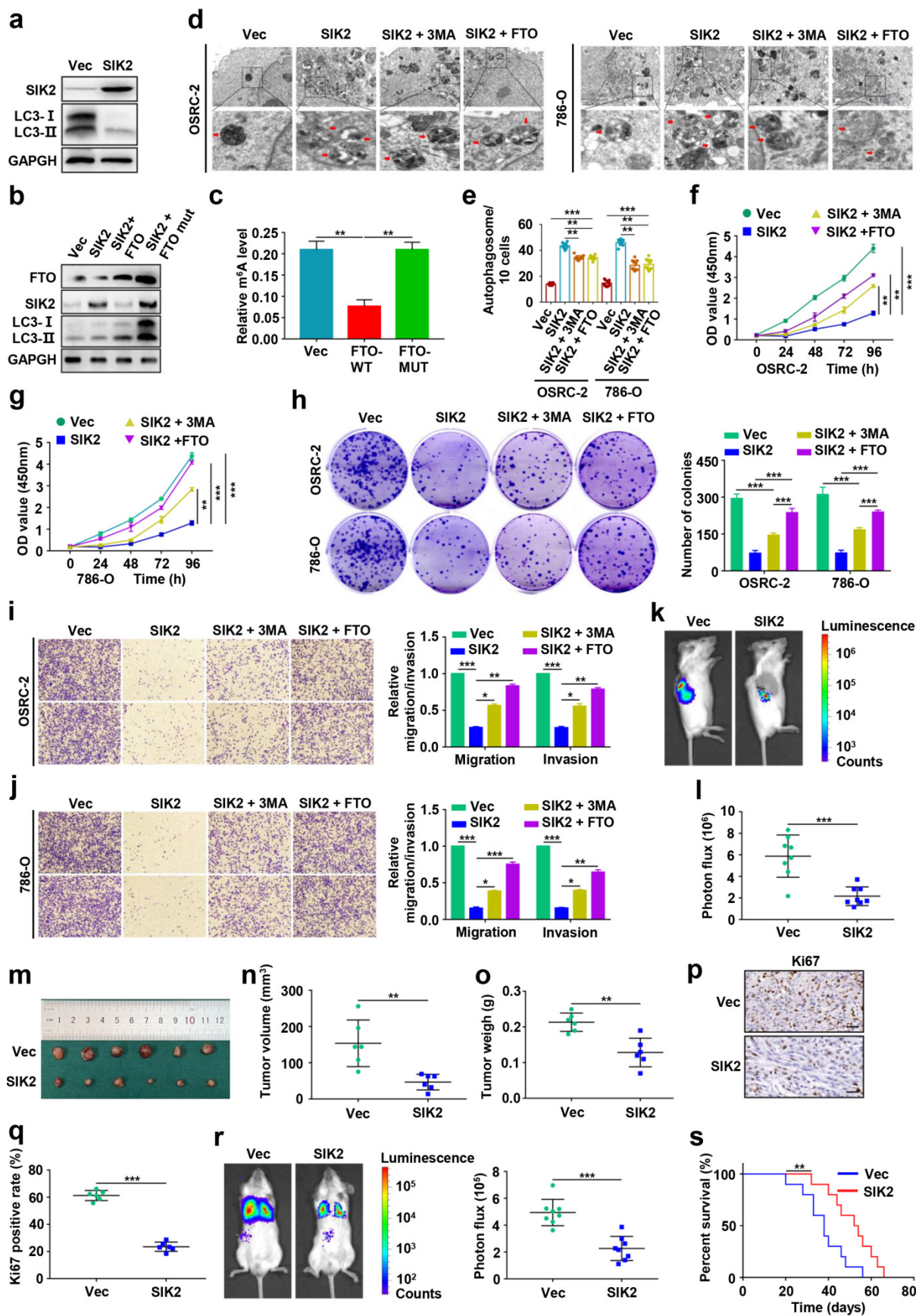


Figure 7. Effects of FTO-mediated SIK2 on autophagic flux, progression and survival in ccRCC. a) Western blot analysis was used to detect SIK2 and LC3- I/II expression in control and SIK2 overexpressing cells. b) Western blot analysis of FTO, SIK2, and LC3- I/II expression in control and SIK2 overexpressed OSRC-2 cells with FTO-WT or FTO-MUT overexpression. c) Quantification of m⁵A levels in vector, FTO-WT, and FTO-MUT by the m⁵A RNA methylation quantification kit. d) TEM demonstrating autophagosomes in control and SIK2 overexpressing OSRC-2 and 786-O cells with 3MA treatment or FTO overexpression. Arrows indicate autophagosomes. Scale bar: 0.5 μ m. e) Quantification of autophagosomes in cells.

f-g) Viability of OSRC-2 and 786-O cells (vector and SIK2, treated with 10 mM 3MA or FTO overexpression) detected using the CCK8 assay. h) Representative images from the colony-forming assay (left panel) and colony number analysis (right panel). All experiments were performed in triplicate and data were presented as the mean \pm SD. i-j) Cell migration and invasion assays of OSRC-2 and 786-O cells after overexpression of FTO (treated with 10 mM 3MA or FTO overexpression). Representative images (left panel) and quantification of the cell migration and invasion assay results (right panel) were shown. k) Representative images of the orthotopic transplantation mouse model (vector and SIK2). l) The analysis of the orthotopic tumor photon flux. m) Image of orthotopic transplanted tumors from the indicated groups. n-o) Tumors were removed 8 weeks after orthotopic transplantation, followed by volume calculation and weight measurement. p-q) Representative IHC staining images of Ki67 (scale bar, 100 μ m) and quantification of Ki67 positive rate. r) Representative images of the orthotopic transplantation lung metastasis mouse model (vector and SIK2; left panel), and the analysis of the lung metastasis photon flux (right panel). s) The survival of mice orthotopically transplanted with control or SIK2 overexpressed OSRC-2 cells was documented (n=10 mice per group). Error bars, SEM; *, $P < 0.05$; **, $P < 0.01$; ***, $P < 0.001$.

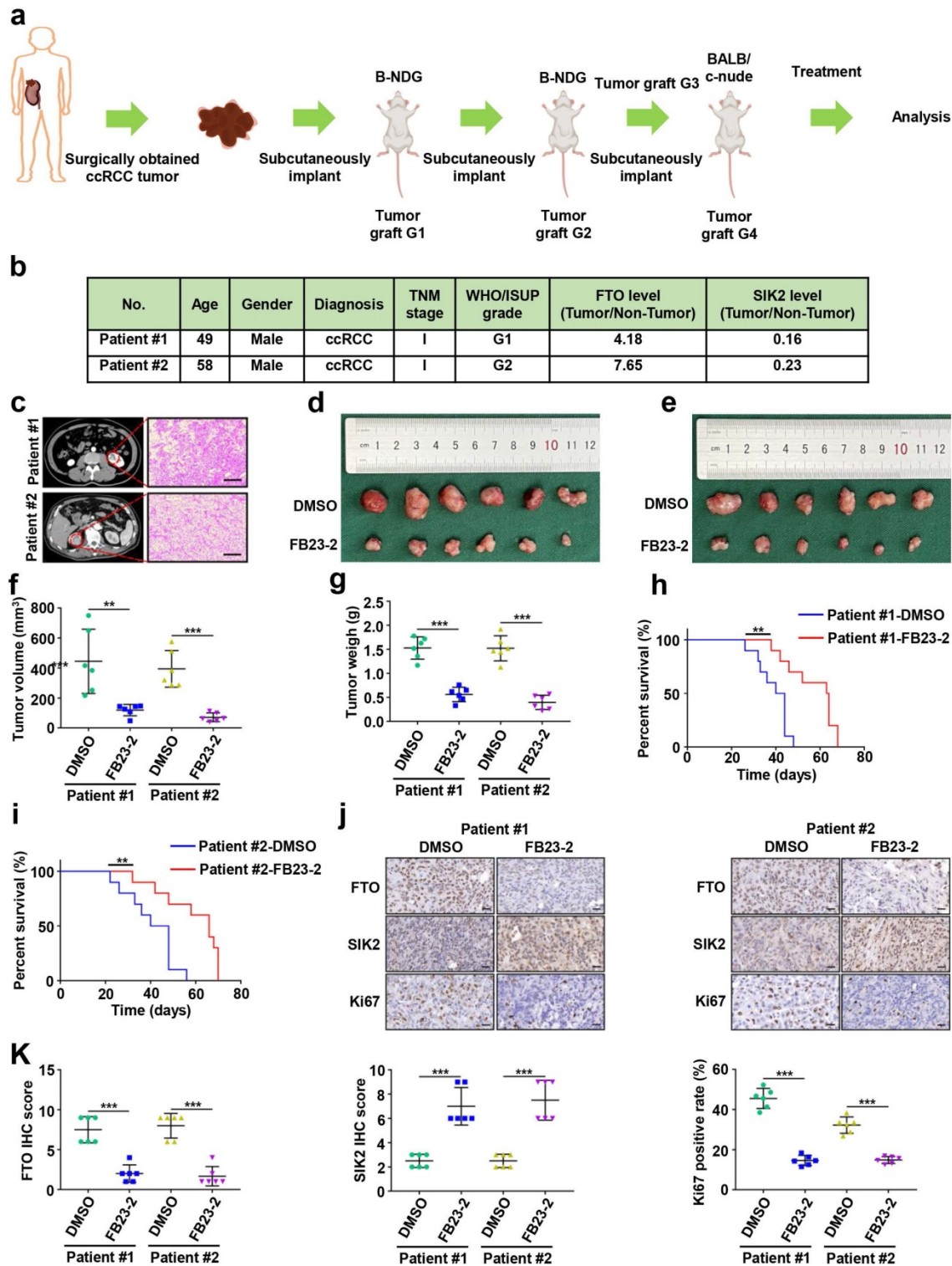


Figure 8. Small-molecule inhibitor targeting FTO exhibits therapeutic efficacy in a patient-derived xenograft (PDX) ccRCC mouse model. a) Graphic illustration of ccRCC PDX mouse models. b) Clinical characteristics of the donor patients. c) Computer tomography (CT) scan and H&E staining of donor patients. Representative images of CT scan (left panel) and H&E staining (right panel). d-e) Harvested PDX tumors in the control and FB23-2 treatment groups. f) Tumor volume of the PDX tumors. g) Tumor weight of the PDX tumors. h-i) The survival of PDX mice treated with DMSO or FB23-2 was documented (n=10 mice per group). j-k) Representative IHC staining images of FTO, SIK2, and Ki67 (scale bar, 100 μ m) and quantification of IHC score. Error bars, SEM; *, $P < 0.01$; ***, $P < 0.001$.

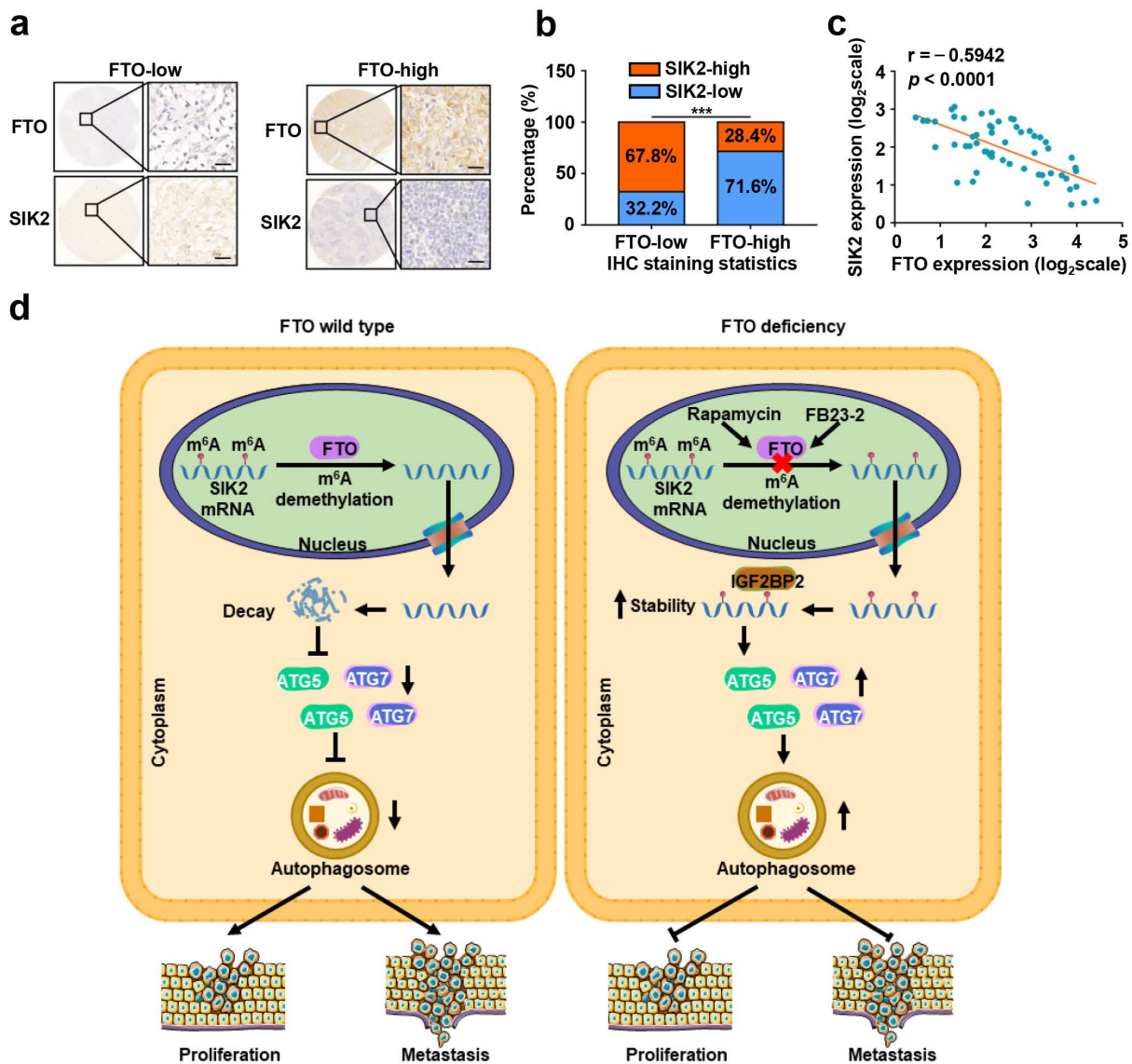


Figure 9. FTO and SIK2 expression is negatively correlated. **a)** Representative IHC staining images of FTO with different dyeing intensity and corresponding SIK2 staining were shown, respectively (scale bar, 100 μ m). **b)** Statistics of IHC staining displayed the percentages of ccRCC specimens with lower or higher FTO expression and corresponding SIK2 levels. **c)** qPCR analysis revealed a negative correlation between FTO and SIK2 expression. **d)** The graphic illustration of FTO-mediated autophagy promoting the progression of ccRCC. Error bars, SEM; $P < 0.001$.

To further assess the clinical significance of FTO-SIK2-autophagy axis promoting ccRCC progression, we examined the expression of FTO and SIK2 in tumor tissues of patients with ccRCC and subsequently categorized the samples into FTO-low and FTO-high groups and determined their relevance in ccRCC. The expression of FTO was negatively correlated with the expression of SIK2 in 60 ccRCC patients (Fig. 9a-b), and the validation of mRNA levels also supported this correlation (Fig. 9c).

Discussion

RNA m⁶A modification has been implicated in the tumorigenesis, progression, and therapeutic response of various tumors, but potent inhibitors targeting m⁶A regulators are still under development.

FTO, one of the key demethylases, has been found to play an oncogenic role in leukemia [29] and oral squamous cell carcinoma [15], and may be a potential therapeutic target. However, the possible role of FTO in ccRCC tumor progression remains unknown. In the present study, we revealed that FTO is an oncogene of ccRCC that mediates autophagy to promote ccRCC progression through the IGF2BP2-SIK2 pathway. More importantly, we validated that the small molecule inhibitor FB23-2 targeting FTO could significantly inhibit tumor growth and prolong the survival time of mice in the PDX model analysis. At the molecular level, rapamycin-induced autophagy attenuates FTO expression at mRNA and protein levels, while silencing FTO suppresses autophagic flux by targeting ATG5 and ATG7. Furthermore, we

identified SIK2 as a critical downstream target of FTO-mediated autophagy, whose mRNA stability is regulated by m⁶A modification through m⁶A reader IGF2BP2 (Fig. 9d). Collectively, these results establish that FTO-autophagy interaction is an epitranscriptional mechanism of ccRCC tumor progression. Our findings are highly significant as they identify for the first time the tumor suppressive role of a small molecule inhibitor targeting FTO in solid tumors and establish a key pathway by which m⁶A modification mediates autophagic flux to modulate tumor progression.

Since the concept of autophagy was introduced by Christian de Duve in 1963 [30], great progress has been made in understanding how autophagy plays a role in physiological and pathological metabolic functions and contributes to improved clinical outcomes. Autophagy occurs at the basal level in all cells and is induced by multiple signals and cellular stresses. Autophagy plays a dual role in the regulation of cancer. On the one hand, it prevents the occurrence of cancer cells, but on the other hand, it is a key mechanism for the survival of cancer cells. Growing evidence suggests that dysregulation of autophagy triggers oncogenic mutations, organelle damage, and accumulation of harmful metabolic molecules that induce oxidative stress, genomic instability, DNA damage, inflammation, and tissue damage, all of which are tumorigenesis inducers [14]. Consistent with the finding of the present study, autophagy was downregulated in multiple types of cancers, suggesting that it has a tumor suppressor role. There are various proteins involved in autophagy regulation, such as Atg4c [31], DAP kinase [32], and PTEN [33], have shown their role in tumor suppression. As a canonical survival pathway, the PI3K-Akt-mTOR signaling axis is activated in various cancers to promote tumor cell proliferation and survival, and the constitutive activation of this axis inhibits autophagy [34]. Thus, identifying therapeutic targets for autophagy in specific tumors is critical for improving patient outcomes.

The regulation of autophagy by m⁶A is dual, m⁶A modification promotes autophagy under certain conditions, but inhibits autophagy activity under other conditions. Recently, studies have demonstrated a close mechanistic correlation between m⁶A RNA methylation and autophagy in tumorigenesis, progression, and response to therapy. The m⁶A methyltransferase METTL13 positively regulates autophagic flux by upregulating the expression of LC3B, ATG5, and ATG7 and plays a key role in β -elemene reversal of gefitinib resistance in non-small cell lung cancer [35]. Li et al. revealed that HIF-1 α -induced YTHDF1 expression promotes the translation

of autophagy-related genes ATG2 and ATG14 in an m⁶A-dependent manner, thereby promoting the progression of hepatocellular carcinoma [19]. These findings undoubtedly greatly increase the understanding of the regulation of tumor cell mechanisms and provide novel ideas for the development of potential therapeutic targets.

Importantly, the m⁶A demethylase FTO has been identified as an essential regulator of m⁶A-autophagy interactions in tumorigenesis. In arsenic-related human skin injury, arsenic stabilizes FTO expression by attenuating p62-mediated selective autophagy, and the upregulation of FTO in turn impairs autophagy, leading to a positive feedback loop that maintains FTO accumulation and induce malignant transformation and tumorigenesis [36]. In human melanoma, metabolic starvation stress regulated by autophagy induces the upregulation of FTO, which in turn promotes tumorigenesis [37]. FTO upregulates ULK1 protein abundance and activates autophagy by reversing m⁶A modification in the 3'-UTR region of ULK1 mRNA, leading to autophagy-mediated tumorigenesis [38]. In epithelial ovarian cancer, FTO binding to circRAB11FIP1 leads to its upregulation, and the induced autophagy accelerates tumorigenesis and progression [39]. Furthermore, our results revealed that rapamycin-induced autophagy activation reduced FTO protein abundance, and FTO-mediated autophagy greatly promoted tumor progression including lung metastasis. These findings highlight the interplay of FTO-mediated mRNA m⁶A modification and autophagy, broadening the multilevel regulation of m⁶A modification in tumor evolution, which is critical for effective therapeutic applications. Our findings are consistent with previous studies confirming that FTO is an oncogene in ccRCC [40]. Overexpressed FTO in ccRCC was identified as a synthetic lethal partner of tumor suppressor gene von Hippel-Lindau (*VHL*) [40], which was also supported by a recent study demonstrating that FTO depletion inhibited ccRCC cells proliferation [41]. However, there was also a report suggesting that FTO made it a tumor suppressor in ccRCC by blocking the FTO-PGC-1 α signaling axis [42]. Elimination of this controversy may need to be clarified in the homogenization model.

To explore the underlying mechanism of m⁶A demethylase FTO-mediated autophagy in ccRCC, we identified SIK2 as a key regulator that plays a decisive role in malignant tumor proliferation and distant metastasis including lung metastasis. Salt-inducible kinase (SIK) was first identified in the adrenal cortex of rats with a high-salt diet, and its three isoforms (SIK1, SIK2, and SIK3) belong to the AMP-activated

protein kinases (AMPKs) family. Among them, SIK2 encodes a protein containing 931 amino acids, and its kinase domain is located in the 20-271 residue region [43]. SIK2 has been reported to be involved in multiple biological roles including malignant progression of ovarian cancer [44], neuronal survival after ischemia [45], and the restriction of intracellular *Salmonella* proliferation [46]. In many human malignancies, SIK2 exhibits significant differential expression, and it plays a key regulatory role involving the PI3K/AKT, AKT/GSK3 β / β -catenin, Hippo-YAP, LKB1-HDAC, and cAMP-PKA pathway. Gao et al. revealed that SIK2 upregulates HIF-1 α and promotes glycolysis by activating the PI3K/AKT signaling pathway in ovarian cancer [47], and SIK2-mediated reprogramming of glucose metabolism enhances ovarian cancer cell proliferation and attenuates apoptosis. Dai et al. found that SIK2 was significantly down-regulated in gastric cancer and inhibited epithelial-mesenchymal transition by inhibiting the AKT/GSK3 β / β -catenin signaling pathway [48]. In addition, the results from Rong et al. suggested that SIK2 expression was positively correlated with breast cancer recurrence, and SIK2 directly phosphorylated LRP6 resulting in activation of Wnt/ β -catenin signaling pathway [49]. However, it is unclear whether SIK2 plays a role in the biological function of ccRCC. Thus, our findings have revealed that SIK2 mRNA stability is regulated by IGF2BP2-dependent pathway, resulting in a regulatory role in FTO-mediated autophagy-related ccRCC malignant progression.

In summary, our results reveal m⁶A modification levels are decreased and closely related to autophagic flux in ccRCC, and we also found that elevated expression of FTO is inhibited by rapamycin treatment, and silencing FTO impairs ccRCC growth and metastasis. Mechanistically, we first identified SIK2 as a functional target of m⁶A-mediated autophagy, thereby prompting FTO to play a conserved and important role in inhibiting autophagy and promoting tumorigenesis through an m⁶A-IGF2BP2 dependent mechanism. Moreover, the small molecule inhibitor FB23-2 targeting FTO inhibited tumor growth in the PDX, suggesting that FTO is a potential therapeutic target for ccRCC. Our findings demonstrate that FTO could be a critical prognostic biomarker and promising therapeutic target in ccRCC.

Abbreviations

ccRCC: clear cell renal cell carcinoma; m⁶A: N⁶-methyladenosine; FTO: fat mass and obesity-associated protein; PDX: patient-derived xenograft; TMA: tissue microarray; qRT-PCR: quantitative

real-time PCR; ATCC: American Type Culture Collection; PBS: phosphate buffered saline; H&E: hematoxylin and eosin; IHC: immunohistochemistry; TEM: transmission electron microscopy; RIP: RNA immunoprecipitation; ANCT: adjacent noncancerous tissue; GFP: green fluorescent protein; mRFP: monomeric red fluorescent protein; TCGA: The Cancer Genome Atlas; OS: overall survival; shRNAs: short hairpin RNAs; MeRIP-seq: methylated RNA immunoprecipitation sequencing; RNA-seq: RNA sequencing; IGF2BP2: insulin-like growth factor 2 mRNA-binding protein 2.

Supplementary Material

Supplementary figures and tables.

<https://www.ijbs.com/v18p5943s1.pdf>

Acknowledgements

Funding

This work was supported by the National High Level Hospital Clinical Research Funding (High Quality Clinical Research Project of Peking University First Hospital, 2022CR75), National Natural Science Foundation of China (No. 82141103; 82172617; 82172665; 81872081), the Scientific Research Seed Fund of Peking University First Hospital (No. 2021SF01), Capital's Funds for Health Improvement and Research (No. 2022-2-4074), Beijing Key Laboratory of Urogenital Diseases (Male) molecular diagnosis and treatment center, and Sino-Russian Mathematics Center.

Ethics Committee Approval

This study was based on guidelines of the Declaration of Helsinki and approved by the Institutional Ethical Board of Peking University First Hospital (Beijing, China, BMU2018JI002). All animal studies in this study were approved by the Laboratory Animal Ethics Committee of Peking University First Hospital (J2022008, Beijing, China), and all details abide by the ethical principles of laboratory animal welfare and was supervised by the committee and laboratory managers.

Author Contributions

Y. Xu: Conceptualization, data curation, formal analysis, validation, investigation, visualization, methodology, writing-original draft, writing-review and editing. J. Zhou: Conceptualization, resources, formal analysis, project administration, writing-review and editing. L. Li: Software, formal analysis, visualization, writing-review and editing. W. Yang: Software, formal analysis, visualization, writing-review and editing. Z. Zhang: Data curation, formal analysis, validation, writing-review and editing. K.

Zhang: Data curation, formal analysis, validation, investigation, writing-review and editing. K. Ma: Software, formal analysis, validation, investigation, visualization, writing-review and editing. H. Xie: Data curation, investigation, writing-review and editing. Z. Z: Resources, supervision, methodology, writing-review and editing. L. Cai: Resources, formal analysis, supervision, methodology, writing-review and editing. Y. Gong: Resources, formal analysis, supervision, methodology, writing-review and editing. K. Gong: Conceptualization, resources, formal analysis, supervision, funding acquisition, writing-original draft, project administration, writing-review and editing. All authors read and approved the final manuscript.

Competing Interests

The authors have declared that no competing interest exists.

References

- Siegel RL, Miller KD, Jemal A. Cancer statistics, 2019. *CA Cancer J Clin.* 2019; 69: 7-34.
- Hsieh JJ, Purdue MP, Signoretti S, et al. Renal cell carcinoma. *Nature reviews Disease primers.* 2017; 3: 17009.
- Marona P, Górka J, Mazurek Z, et al. MCP1 Downregulation in Clear Cell Renal Cell Carcinoma Promotes Vascularization and Metastatic Progression. *Cancer research.* 2017; 77: 4905-20.
- Shen H, Laird PW. Interplay between the cancer genome and epigenome. *Cell.* 2013; 153: 38-55.
- Wang X, Lu Z, Gomez A, et al. N6-methyladenosine-dependent regulation of messenger RNA stability. *Nature.* 2014; 505: 117-20.
- Huang Y, Su R, Sheng Y, et al. Small-Molecule Targeting of Oncogenic FTO Demethylase in Acute Myeloid Leukemia. *Cancer Cell.* 2019; 35: 677-91.e10.
- Deng X, Su R, Weng H, et al. RNA N(6)-methyladenosine modification in cancers: current status and perspectives. *Cell research.* 2018; 28: 507-17.
- Wang X, Wu R, Liu Y, et al. m(6)A mRNA methylation controls autophagy and adipogenesis by targeting Atg5 and Atg7. *Autophagy.* 2020; 16: 1221-35.
- Jacobsson JA, Schiöth HB, Fredriksson R. The impact of intronic single nucleotide polymorphisms and ethnic diversity for studies on the obesity gene FTO. *Obesity reviews : an official journal of the International Association for the Study of Obesity.* 2012; 13: 1096-109.
- Li J, Han Y, Zhang H, et al. The m6A demethylase FTO promotes the growth of lung cancer cells by regulating the m6A level of USP7 mRNA. *Biochemical and biophysical research communications.* 2019; 512: 479-85.
- Liu S, Huang M, Chen Z, et al. FTO promotes cell proliferation and migration in esophageal squamous cell carcinoma through up-regulation of MMP13. *Experimental cell research.* 2020; 389: 111894.
- Xu D, Shao W, Jiang Y, et al. FTO expression is associated with the occurrence of gastric cancer and prognosis. *Oncology reports.* 2017; 38: 2285-92.
- Li Z, Weng H, Su R, et al. FTO Plays an Oncogenic Role in Acute Myeloid Leukemia as a N(6)-Methyladenosine RNA Demethylase. *Cancer Cell.* 2017; 31: 127-41.
- Levine B. *Cell biology: autophagy and cancer.* Nature. 2007; 446: 745-7.
- Wang F, Liao Y, Zhang M, et al. N6-methyladenosine demethyltransferase FTO-mediated autophagy in malignant development of oral squamous cell carcinoma. *Oncogene.* 2021; 40: 3885-98.
- Zuo X, Chen Z, Cai J, et al. 5-Hydroxytryptamine Receptor 1D Aggravates Hepatocellular Carcinoma Progression Through FoxO6 in AKT-Dependent and Independent Manners. *Hepatology (Baltimore, Md).* 2019; 69: 2031-47.
- Chen Y, Wang J, Xu D, et al. m(6)A mRNA methylation regulates testosterone synthesis through modulating autophagy in Leydig cells. *Autophagy.* 2021; 17: 457-75.
- Shi H, Wang X, Lu Z, et al. YTHDF3 facilitates translation and decay of N(6)-methyladenosine-modified RNA. *Cell research.* 2017; 27: 315-28.
- Li Q, Ni Y, Zhang L, et al. HIF-1 α -induced expression of m6A reader YTHDF1 drives hypoxia-induced autophagy and malignancy of hepatocellular carcinoma by promoting ATG2A and ATG14 translation. *Signal transduction and targeted therapy.* 2021; 6: 76.
- Frye M, Harada BT, Behm M, et al. RNA modifications modulate gene expression during development. *Science (New York, NY).* 2018; 361: 1346-9.
- Ho TH, Serie DJ, Parasramka M, et al. Differential gene expression profiling of matched primary renal cell carcinoma and metastases reveals upregulation of extracellular matrix genes. *Ann Oncol.* 2017; 28: 604-10.
- López-Lago MA, Thodima VJ, Guttapalli A, et al. Genomic deregulation during metastasis of renal cell carcinoma implements a myofibroblast-like program of gene expression. *Cancer research.* 2010; 70: 9682-92.
- Li J, Xie H, Ying Y, et al. YTHDF2 mediates the mRNA degradation of the tumor suppressors to induce AKT phosphorylation in N6-methyladenosine-dependent way in prostate cancer. *Mol Cancer.* 2020; 19: 152.
- Hou G, Zhao X, Li L, et al. SUMOylation of YTHDF2 promotes mRNA degradation and cancer progression by increasing its binding affinity with m6A-modified mRNAs. *Nucleic acids research.* 2021; 49: 2859-77.
- Wang X, Ji Y, Feng P, et al. The m6A Reader IGF2BP2 Regulates Macrophage Phenotypic Activation and Inflammatory Diseases by Stabilizing TSC1 and PPAR γ . *Advanced science (Weinheim, Baden-Württemberg, Germany).* 2021; 8: 2100209.
- Han Z, Niu T, Chang J, et al. Crystal structure of the FTO protein reveals basis for its substrate specificity. *Nature.* 2010; 464: 1205-9.
- Liu Y, Liang G, Xu H, et al. Tumors exploit FTO-mediated regulation of glycolytic metabolism to evade immune surveillance. *Cell metabolism.* 2021; 33: 1221-33.e11.
- Su R, Dong L, Li C, et al. R-2HG Exhibits Anti-tumor Activity by Targeting FTO/m(6)A/MYC/CEBPA Signaling. *Cell.* 2018; 172: 90-105.e23.
- Su R, Dong L, Li Y, et al. Targeting FTO Suppresses Cancer Stem Cell Maintenance and Immune Evasion. *Cancer Cell.* 2020; 38: 79-96.e11.
- Klionsky DJ. Autophagy revisited: a conversation with Christian de Duve. *Autophagy.* 2008; 4: 740-3.
- Mariño G, Salvador-Montoliu N, Fueyo A, et al. Tissue-specific autophagy alterations and increased tumorigenesis in mice deficient in Atg4C/autophagin-3. *The Journal of biological chemistry.* 2007; 282: 18573-83.
- Bialik S, Kimchi A. Lethal weapons: DAP-kinase, autophagy and cell death: DAP-kinase regulates autophagy. *Current opinion in cell biology.* 2010; 22: 199-205.
- Rusten TE, Lindmo K, Juhász G, et al. Programmed autophagy in the Drosophila fat body is induced by ecdysone through regulation of the PI3K pathway. *Developmental cell.* 2004; 7: 179-92.
- LoPiccolo J, Blumenthal GM, Bernstein WB, et al. Targeting the PI3K/Akt/mTOR pathway: effective combinations and clinical considerations. *Drug resistance updates : reviews and commentaries in antimicrobial and anticancer chemotherapy.* 2008; 11: 32-50.
- Liu S, Li Q, Li G, et al. The mechanism of m(6)A methyltransferase METTL3-mediated autophagy in reversing gefitinib resistance in NSCLC cells by β -elemene. *Cell death & disease.* 2020; 11: 969.
- Cui YH, Yang S, Wei J, et al. Autophagy of the m(6)A mRNA demethylase FTO is impaired by low-level arsenic exposure to promote tumorigenesis. *Nature communications.* 2021; 12: 2183.
- Yang S, Wei J, Cui YH, Park G, Shah P, Deng Y, et al. m(6)A mRNA demethylase FTO regulates melanoma tumorigenicity and response to anti-PD-1 blockade. *Nature communications.* 2019; 10: 2782.
- Jin S, Zhang X, Miao Y, et al. m(6)A RNA modification controls autophagy through upregulating ULK1 protein abundance. *Cell research.* 2018; 28: 955-7.
- Zhang Z, Zhu H, Hu J. CircRAB11FIP1 promoted autophagy flux of ovarian cancer through DSC1 and miR-129. *Cell death & disease.* 2021; 12: 219.
- Xiao Y, Thakkar KN, Zhao H, et al. The m(6)A RNA demethylase FTO is a HIF-independent synthetic lethal partner with the VHL tumor suppressor. *Proceedings of the National Academy of Sciences of the United States of America.* 2020; 117: 21441-9.
- Zhang C, Chen L, Lou W, et al. Aberrant activation of m6A demethylase FTO renders HIF2 α (low/-) clear cell renal cell carcinoma sensitive to BRD9 inhibitors. *Science translational medicine.* 2021; 13: eabf6045.
- Zhuang C, Zhuang C, Luo X, et al. N6-methyladenosine demethylase FTO suppresses clear cell renal cell carcinoma through a novel

- FTO-PGC-1 α signalling axis. *Journal of cellular and molecular medicine*. 2019; 23: 2163-73.
43. Katoh Y, Takemori H, Horike N, et al. Salt-inducible kinase (SIK) isoforms: their involvement in steroidogenesis and adipogenesis. *Molecular and cellular endocrinology*. 2004; 217: 109-12.
 44. Miranda F, Mannion D, Liu S, et al. Salt-Inducible Kinase 2 Couples Ovarian Cancer Cell Metabolism with Survival at the Adipocyte-Rich Metastatic Niche. *Cancer Cell*. 2016; 30: 273-89.
 45. Sasaki T, Takemori H, Yagita Y, et al. SIK2 is a key regulator for neuronal survival after ischemia via TORC1-CREB. *Neuron*. 2011; 69: 106-19.
 46. Hahn M, Covarrubias-Pinto A, Herhaus L, et al. SIK2 orchestrates actin-dependent host response upon *Salmonella* infection. *Proceedings of the National Academy of Sciences of the United States of America*. 2021; 118.
 47. Gao T, Zhang X, Zhao J, et al. SIK2 promotes reprogramming of glucose metabolism through PI3K/AKT/HIF-1 α pathway and Drp1-mediated mitochondrial fission in ovarian cancer. *Cancer Lett*. 2020; 469: 89-101.
 48. Dai XM, Zhang YH, Lin XH, et al. SIK2 represses AKT/GSK3 β / β -catenin signaling and suppresses gastric cancer by inhibiting autophagic degradation of protein phosphatases. *Molecular oncology*. 2021; 15: 228-45.
 49. Rong Z, Zhang L, Li Z, et al. SIK2 maintains breast cancer stemness by phosphorylating LRP6 and activating Wnt/ β -catenin signaling. *Oncogene*. 2022; 41: 2390-403.